




## Fractal and Conventional Analysis of Cu Content Effect on the Microstructure of Al-Si-Cu-Mg Alloys

Bertha Y. Casas<sup>a</sup>, Juan C. Carranza<sup>a</sup> , Ignacio A. Figueroa<sup>b</sup> , Jose G. González<sup>b</sup>,  
Orlando Hernández<sup>c</sup>, Luis Béjar<sup>d</sup>, Claudio Aguilar<sup>e</sup>, Ismeli Alfonso<sup>a\*</sup> 

<sup>a</sup>Universidad Nacional Autónoma de México, Instituto de Investigaciones en Materiales, Unidad Morelia, Morelia, Michoacán, México

<sup>b</sup>Universidad Nacional Autónoma de México, Instituto de Investigaciones en Materiales, Ciudad de México, México

<sup>c</sup>Universidad Nacional Autónoma de México, Escuela Nacional de Estudios Superiores, Morelia, Michoacán, México

<sup>d</sup>Universidad Michoacana de San Nicolás de Hidalgo, Facultad de Ingeniería Mecánica, Morelia, Michoacán, México

<sup>e</sup>Universidad Técnica Federico Santa María, Department of Metallurgical and Materials Engineering, Valparaíso, Chile

Received: December 08, 2019; Revised: July 01, 2020; Accepted: July 11, 2020

This work analyzes the effect of Cu additions on the microstructure of quaternary alloys Al-6Si-7Mg-xCu (x= 3, 5 and 7 wt.%) produced by conventional metallurgy. Microstructural modifications were studied using Optical Microscopy (OM), X-Ray Diffraction (XRD) and Scanning Electron Microscopy (SEM), focusing on second phases identification and quantification. Conventional image analyses were developed measuring the total percentage of second phases, and individually for each phase determining its equivalent diameter, shape factor, roundness and aspect ratio; while fractal analyses were carried out complementarily through fractal dimension measurements for the whole microstructure and for individual phases. Compression tests were also carried out. SEM and XRD results revealed that second phases were eutectic Si, Mg<sub>2</sub>Si, Al<sub>2</sub>Cu and Al<sub>5</sub>Cu<sub>2</sub>Mg<sub>8</sub>Si<sub>6</sub> (Q). The increase in Cu content led to higher quantities of these phases, mainly Al<sub>2</sub>Cu, which was barely present for the alloy with the lowest Cu content. Morphologies of second phases depended on Cu content, being present as eutectic, block like, finely dispersed or primary particles. The combination of conventional and fractal parameters provided a useful tool for comparatively analyze microstructural modifications and second phases features. It was also found that the compressive behavior of the alloys depended on the resulting microstructures.

**Keywords:** Al alloys, microstructure, mechanical properties, SEM, fractal, second phases.

### 1. Introduction

Research focused on aluminum alloys has been developed in an uninterrupted way in the last years, been published many works mainly related to microstructural modifications, which derivate from the presence of different second phases with a wide variety of morphologies, i.e. block-like, fibrillar, particulate, acicular, Chinese script, etc<sup>1-4</sup>. The presence of these phases in Al alloys directly depends on alloying elements content and manufacturing process, affecting their final mechanical properties. Among these alloys is the quaternary Al-Si-Cu-Mg system, whose microstructure is composed by eutectic Si, Q (Al<sub>5</sub>Mg<sub>8</sub>Cu<sub>2</sub>Si<sub>6</sub>), Al<sub>2</sub>Cu and Mg<sub>2</sub>Si, in addition to other complex intermetallic compounds<sup>1,5-8</sup>. These alloys have Si contents between 5.5 and 6.5 wt.% and Cu from 3.0 to 4.0%. In search of significant microstructural modifications, previous works have studied Mg contents between 3 and 11%<sup>5,8</sup>. This element led to the formation of

high quantity of Mg<sub>2</sub>Si, also modifying Cu-rich phases from Al<sub>2</sub>Cu to Q (Al<sub>5</sub>Mg<sub>8</sub>Cu<sub>2</sub>Si<sub>6</sub>)<sup>1-5</sup>. If Cu content is significantly increased it is expected a contrary effect, modifying Cu-rich phases from Q to Al<sub>2</sub>Cu. In the case of Cu, contents no higher than approximately 4.0 have been studied for this alloy system while Mg content is increased. The study of such phase transformations is necessary for finding new applications of these alloys. Besides, second phases are directly related to one of the new applications of Al alloys: their foams. These relatively new kind of materials have combinations of mechanical, thermal, acoustic, electrical and chemical properties that boost their use. These properties motivate their applications as automotive parts, energy absorbers, dust and fluid filters, heat exchangers, catalysis supports and sound absorbers<sup>9-11</sup>.

Although metallic foams are generally manufactured using methods such as infiltration of liquid metal, powder metallurgy and liquid processes<sup>9-11</sup>, a solid-state method has

\*e-mail: [ialfonso@unam.mx](mailto:ialfonso@unam.mx)

been previously reported for Al alloys, generating connected or non-connected pores, depending on the alloy system<sup>5,12</sup>. This process uses over-heat-treatments at temperatures higher than incipient melting points of second phases, leading to peritectic reactions that provokes pores formation. Then, the study of second phases features is essential for a better understanding of this process. For second phases with regular shapes such as circles, needles, polygons, etc., it is easy to determine their sizes and morphologies. Among the parameters that could be used for these purposes is equivalent diameter ( $D_e$ ), defined as the diameter of a circle with equivalent area ( $A_p$ ) in Equation 1<sup>13,14</sup>. It is used since it is common to analyze particles as if they were spheres.

$$D_e = \left( \frac{4A_p}{\pi} \right)^{1/2} \quad (1)$$

Another common parameter is aspect ratio ( $AR$ ), which represents the ratio between the length and the width (or major axis/minor axis,  $L/W$ ), also represented using roundness or chunkiness,  $R$ , which is the inverse of the aspect ratio, and defined in Equation 2<sup>14</sup>.

$$R = l / AR = \frac{4A_p}{\pi L_p^2} \quad (2)$$

Shape factor,  $F$  (also known as circularity)<sup>14</sup>, is another dimensionless parameter also used for analyzing second phases, defined in Equation 3 (where  $P_p$  is the perimeter). A perfect circle will have a shape factor of 1.0, while a value near 0 indicates an irregular or elongated shape.

$$F = \frac{4\pi A_p}{P_p^2} \quad (3)$$

These parameters are easy to determine for particles with shapes close to the spherical, and their estimations using image analysis agree well with experimental determinations. Although  $R$  is well defined for shapes as ideal cone ( $R = 0.794$ ), cube ( $R = 0.806$ ), or ideal cylinder ( $R = 0.874$ ), particle shape strongly affects measurements for non-spherical particles, been necessary to introduce corrections between experimental and image analysis determinations<sup>14</sup>. For non-particulate phases with irregular shapes, such as fibrillar or Chinese script, this problem increases because their shapes are too much far from the used premise of “analyze particles as if they were spheres”. That is why image analysis of Al alloys has been mainly focused on the percentage of phases and the size of particles, as the case of intermetallic<sup>15</sup> or eutectic Si particles<sup>16</sup>; or circularity determinations as the work of Krupiński et al.<sup>17</sup>, who analyzed the average perimeter to surface ratio of phases in an Al-Si-Cu alloy<sup>16</sup>.

A parameter previously used for characterizing complex phases is the fractal dimension ( $D_f$ ), not only for Al alloys<sup>1,18,19</sup> but also for other materials with inclusions, as tourmalines in minerals<sup>20</sup>.  $D_f$  is a measure of a geometry complexity: larger

the dimension, the more heterogeneous and complex the fractal object is. Fractals is a non-Euclidean geometry theory used to describe the irregularity in nature<sup>21</sup>. The magnitude of  $D_f$  is very easy to measure using the box-counting method, being a global analysis of the geometry obtained by plotting  $N(\delta)$  against  $\delta$  in a log-log scale according to:

$$D_f = \lim_{\delta \rightarrow 0} \log N(\delta) / \log \delta \quad (4)$$

where  $\delta$  is the magnification factor or scale (corresponding to the inverse of the grid size  $l$ ) and  $N(\delta)$  is the number of self-similar parts under the fixed magnification factor. A first step for measuring  $D_f$  and the above-mentioned parameters ( $D_e$ ,  $R$  and  $F$ ) is the use of image analysis of micrographs obtained using different characterization techniques, e.g. OM and SEM. The accuracy of their determinations depends on the sample preparation, the characterization technique, and the method used for processing the images. These methods are mainly based on the identification of isolated regions in a binary image, segmenting it so that black pixels represent second phases<sup>22</sup>. Due to the complexity of the microstructure for quaternary aluminum alloys, as the case of the Al-Si-Cu-Mg system, their fractal analysis could be a complementary tool for the study of their phases features. That is why the main objective of the present paper is to study from conventional and fractal points of view the microstructural modifications originated due to the increase in Cu content for three Al-Si-Cu-Mg alloys.

## 2. Experimental

Three experimental Al-6Si-7Mg-xCu ( $x = 3\%$ ,  $5\%$  and  $7 \text{ wt.}\%$ ) alloys were produced in a Leybold-Heraeus induction furnace without controlled atmosphere, using Al, Cu, Mg and Si of high purity (99.8%). A graphite crucible was used, while melting temperature was kept at  $750 \text{ }^\circ\text{C} \pm 10 \text{ }^\circ\text{C}$ . The molten alloys were poured into conventional cylindrical molds to obtain bars of 11 cm in height and 6 cm in diameter. Resulting chemical compositions can be seen in Table 1. As already mentioned, the aim of using high Cu contents is to increase Cu-rich phases and analyze the possibility of manufacturing foams using over-heat-treatments.

Cubic-shaped samples of 2.0 cm were sectioned from each alloy ingot and polished using standard metallographic techniques, followed by their microstructural characterization by OM and SEM using respectively a LABOMED MET 400 OM and a JEOL JSM IT300 scanning electron microscope operated at 20 kV, with a BRUKER XFlash6130 energy dispersive X-ray spectrometer (EDX) attached. EDX helped to phases identification, fact that was supported by X-ray diffractometry through a Bruker D8 Advance XRD with  $\text{CuK}\alpha$  radiation ( $\lambda = 1.54 \text{ \AA}$ ) at 30 kV and 25 mA. To ensure repetitive and accurate results 3 samples were analyzed by microscopy techniques for each condition, while for a better statistical analysis 5 images were obtained from

**Table 1.** Chemical composition (in wt.%) of the experimental alloys.

| Alloy | Si   | Cu   | Mg   | Fe   | Mn   | Zn   | Al      |
|-------|------|------|------|------|------|------|---------|
| Cu3   | 6.11 | 3.18 | 7.22 | 0.02 | 0.01 | 0.01 | Balance |
| Cu5   | 6.22 | 5.08 | 6.91 | 0.02 | 0.01 | 0.01 | Balance |
| Cu7   | 5.88 | 7.06 | 7.20 | 0.01 | 0.01 | 0.01 | Balance |

different zones for each sample. Microstructures captured by these techniques were analyzed through ImageJ<sup>23</sup>, determining area percentage,  $D_e$ ,  $R$ ,  $F$  and  $D_f$  using the tools integrated to this software. Compression tests were conducted on an Instron 1125-5500R materials testing machine with a crosshead speed of 0.5 mm/min, according to ASTM E9-09 “Standard Test Methods of Compression Testing of Metallic Materials at Room Temperature”, using cylindrical samples of 19 mm diameter and 15 mm in length. Compression test instead of tension was selected

considering the desired future application of these alloys for manufacturing foams in-situ.

### 3. Results and Discussion

#### 3.1 Microstructural analysis

Important microstructural modifications were produced when Cu content increased, as can be observed in Figure 1 a-c. This figure shows backscattered (BE) SEM micrographs of

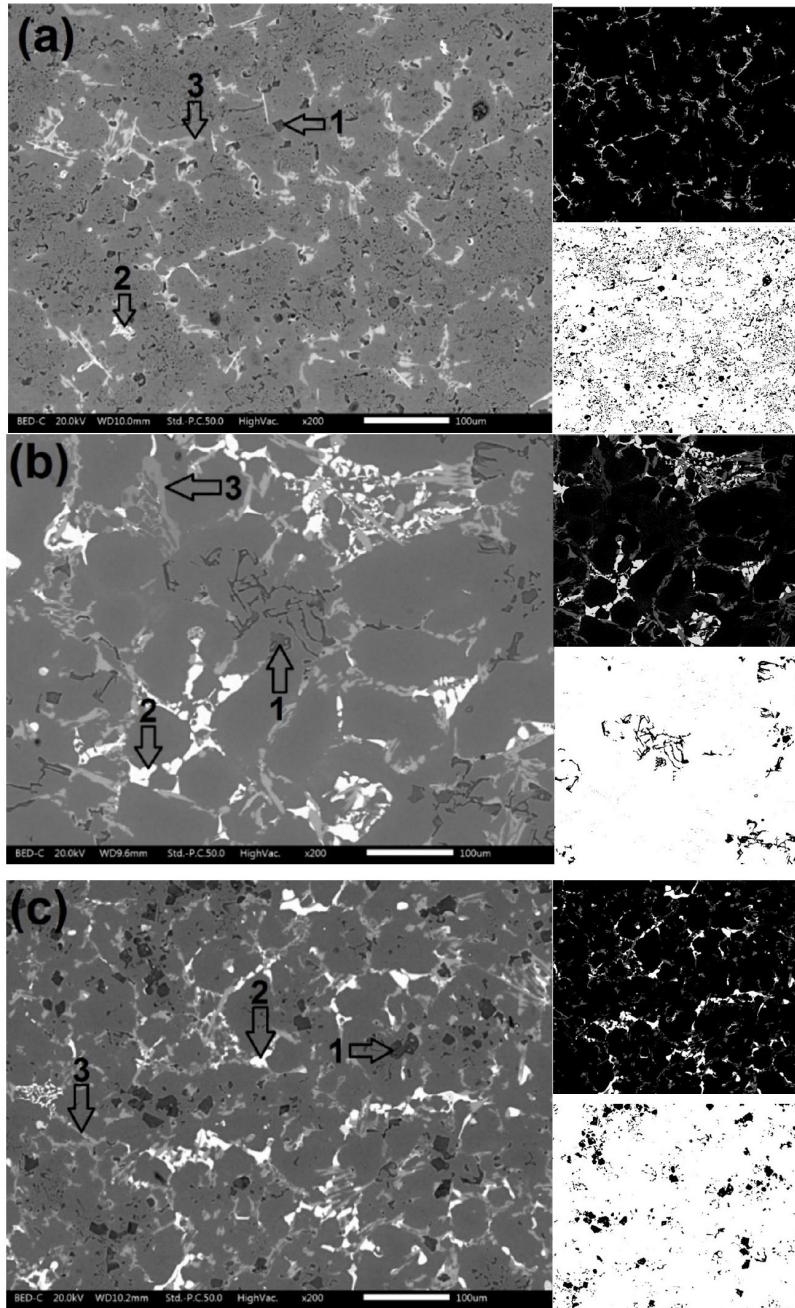


**Figure 1.** BE-SEM micrographs of the experimental alloys with Cu contents of: (a) 3%, (b) 5%, and (c) 7%. Arrows indicate visible second phases: (1)  $Mg_2Si$ , (2)  $Al_2Cu$ , and (3)  $Al_3Cu_2Mg_8Si_6$ . Images modified using ImageJ are observed to the right sides for Cu-rich phases (top) and  $Mg_2Si$  (down).



the three experimental alloys. Images modified using ImageJ are observed to the right side of SEM images, remarking Cu-rich phases (top) and  $Mg_2Si$  (down). As a first overview, and according to literature and our previous works<sup>1,3,5</sup>, it can be observed that for the alloy with 3% Cu (Figure 1a) besides  $\alpha$ -Al there are present two phases: i) Cu-rich phases (mainly light grey Q phase, and low quantity of white  $Al_2Cu$ ), and ii)  $Mg_2Si$  (black), mainly eutectic. Few spaces free of second phases are observable ( $\alpha$ -Al solid solution). Cu-rich phases are represented in the modified image also as white in the black background, while  $Mg_2Si$  is represented as black in the other modified image with white background. As can be observed, these modified images are a very useful tool for the study of the microstructure of Al alloys. For the alloy with 5% of Cu (Cu5) microstructure (see Figure 1b) is quite different from the alloy Cu3, predominating block-like Cu-rich phases of sizes significantly higher. For this alloy the content of  $Al_2Cu$  significantly increased, while  $Mg_2Si$  presents a morphology different compared to Figure 1a because it is markedly irregular and seems to be isolated parts of agglomerates similar to Chinese scripts<sup>5</sup>. Another important difference for this alloy is the presence of important second phases free

zones. Modified images clearly show these features. Finally, for the alloy with 7% Cu (see Figure 1c)  $Mg_2Si$  is present mainly as primary particles (although eutectic  $Mg_2Si$  is also observed), while again the quantities of Q and  $Al_2Cu$  are high. The presence of second phases free zones is also observed, but of lower extension compared to alloy Cu5. Modified images help to this observation. The increase in Cu content for alloys Cu5 and Cu7 favored the formation of  $Al_2Cu$  due to the availability of this element in the molten liquid, not enough in the alloy with 3% Cu, just precipitating Q phase from liquid. It is reported that the solidification of these second phases begins between 577 and 599 °C with primary  $Mg_2Si$ , followed by eutectic  $Mg_2Si$ , Q +  $Al_2Cu$  (below 546 °C)<sup>24</sup>.

Due to the particularities of the alloy system under study and for a better microstructural observation, OM and SEM techniques were used. It is necessary a combination of both kind of images because not all the phases can be easily resolved using only one technique, e.g.  $Al_2Cu$  appears slightly darker than  $\alpha$ -Al in OM images, while eutectic Si is almost impossible to differentiate in SEM images. Thus, microstructures obtained using these two techniques are presented in Figures 2a-f to Figure 4a-f, also including SEM

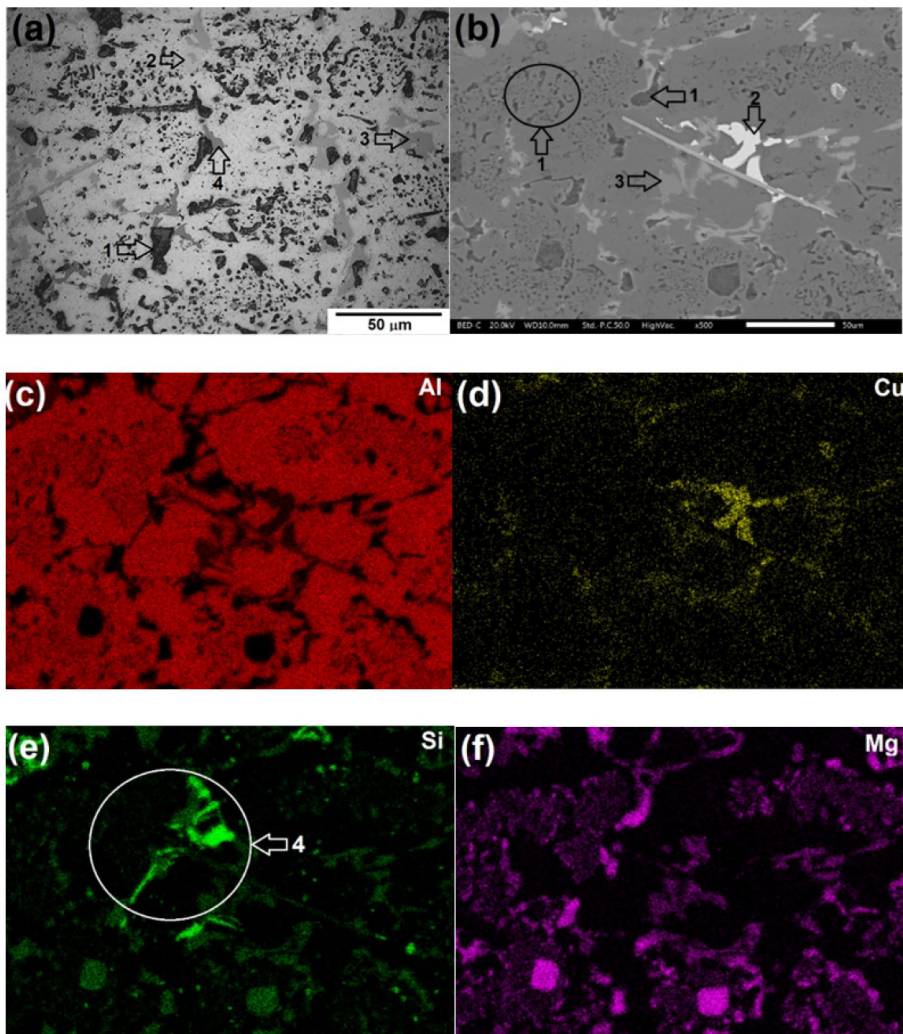


**Figure 2.** OM (a) and BE-SEM (b) micrographs of the experimental alloys with Cu content of 3%, and EDX-mappings corresponding to Al (c), Cu (d), Si (e) and Mg (f). Arrows indicate second phases: (1)  $Mg_2Si$ , (2)  $Al_2Cu$ , (3)  $Al_3Cu_2Mg_8Si_6$ , and (4) Si eutectic.

EDX mappings. These techniques allowed the study of all the phases, being an excellent tool to determine semi-quantitatively their chemical composition, which can be finally proved by XRD. Besides, EDX mapping can resolve images where second phases are barely observable due to their atomic numbers similar to matrix (as eutectic Si). By the other hand, BE-SEM image mode easily resolves phases with elements whose atomic numbers are far different from matrix (as  $Mg_2Si$ , which is almost black due to the small atomic number of Mg; or Cu-rich phases, light grey or white due to the high atomic number of Cu). The combination of these image modes is presented in Figure 2a-f for the alloy Cu3. There can be observed Si and  $Mg_2Si$  eutectics (predominant second phase), few primary  $Mg_2Si$  particles, and block-like Q and  $Al_2Cu$ . The percentages of these phases can be observed in Table 2, with a total of 18.30%. As above mentioned, eutectic Si is not observed in SEM images (Figure 2b), being necessary EDX mapping (see Figure 2e, circled);

while  $Al_2Cu$  is barely observable in the OM micrograph of Figure 2a because it is slightly darker than  $\alpha$ -Al matrix. These results demonstrate the importance of combining SEM and OM, besides EDX mapping. Due to the quantity of each element in the phases, mapping for Cu is more intense for  $Al_2Cu$  than for Q phases (Figure 2d); being also more intense Si for eutectic Si than for  $Mg_2Si$  (Figure 2e); and Mg for primary particles than for  $Mg_2Si$ . Average  $D_e$  for  $Mg_2Si$  isolated black phases in Figures 2a and 2b (parts of the eutectic) is  $6.8 \pm 0.9 \mu m$ , presenting an aspect ratio near 1. Otherwise, eutectic Si has  $D_e = 9.6 \pm 1.1 \mu m$  and aspect ratio of 1.3; and for Cu-rich phases  $D_e = 13.5 \pm 1.3 \mu m$  and aspect ratio 1.4. These phases were already reported in detail in a previous work<sup>5</sup> for alloys with different Mg contents. XRD analyses that will be further presented contributed to the identification presented in Figure 2a-f.

Microstructure for the alloy Cu5 is quite different from the alloy Cu3, fact that can be observed in Figure 3a-f.

**Table 2.** Second phases percentage for the experimental alloys.

| Alloy/Phase | $Mg_2Si$         | $Al_2Cu$        | Q               | Si              | Total            |
|-------------|------------------|-----------------|-----------------|-----------------|------------------|
| Cu3         | $10.00 \pm 0.81$ | $0.80 \pm 0.09$ | $6.58 \pm 0.84$ | $0.92 \pm 0.06$ | $18.30 \pm 1.66$ |
| Cu5         | $5.70 \pm 1.11$  | $6.01 \pm 0.93$ | $9.20 \pm 1.56$ | $0.11 \pm 0.01$ | $21.02 \pm 2.61$ |
| Cu7         | $7.00 \pm 1.08$  | $8.80 \pm 1.05$ | $7.09 \pm 1.27$ | 0               | $22.89 \pm 2.40$ |

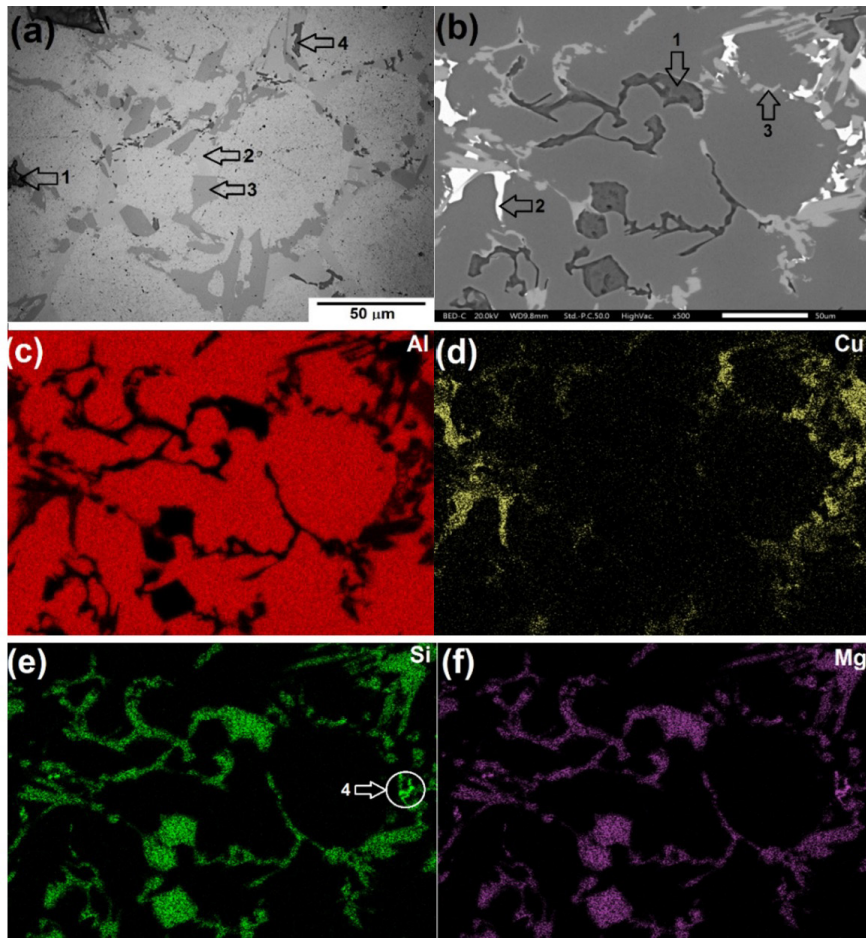


**Figure 3.** OM (a) and BE-SEM (b) micrographs of the experimental alloys with Cu content of 5%, and EDX-mappings corresponding to Al (c), Cu (d), Si (e) and Mg (f). Arrows indicate second phases: (1)  $Mg_2Si$ , (2)  $Al_2Cu$ , (3)  $Al_3Cu_2Mg_8Si_6$ , and (4) Si eutectic.



The total quantity of second phases reached 21.02%, now Q is the predominant phase, but  $\text{Al}_2\text{Cu}$  content increased to 6%, almost the same that for  $\text{Mg}_2\text{Si}$  (phase whose content decreased). The increase in the quantity of Cu-rich phases was influenced by the increase in Cu content in the molten material, which modified the Si:Cu:Mg ratio from 2:1:2.3 to 1.2:1:1.4, favoring Cu-rich phases formation, mainly Q. This phase contains high Mg and Si percentages, reducing the quantities of these elements for the formation of  $\text{Mg}_2\text{Si}$ . In the alloy with 3%Cu Si:Mg ratio was near 1, but Si:Cu and Mg:Cu ratios were  $\sim 2$ , favoring  $\text{Mg}_2\text{Si}$  formation due to the insufficient quantity of Cu for the formation of  $\text{Al}_2\text{Cu}$ . Cu-rich phases are similar to the observed in Figure 2b, but with the important difference that their sizes are significantly higher ( $D_e = 24.5 \pm 1.8 \mu\text{m}$  and aspect ratio of 1.8). This led to the presence of important second

phases free zones of average sizes of  $74 \pm 11 \mu\text{m}$ .  $\text{Mg}_2\text{Si}$  is different from the observed for the alloy Cu3 because it is composed by large parts instead isolated particles as the already observed in Figure 2a. Contrarily to the observed for the alloy Cu3, no differences in Mg intensities were observed in EDX of Figure 3f, fact that could indicate that there is only one phase. For this alloy the quantity of Si eutectic is very low, and just small spots are visible, as is observed in Figure 3a or in mapping of Si (see circled in Figure 3e).

Finally, the microstructure for the alloy Cu7 can be observed in Figure 4e-f. The most important modifications are again related to the increase in the total quantity of second phases, reaching 22.89%, also predominating Cu-rich phases, but in this case  $\text{Al}_2\text{Cu}$  (see Table 2).  $\text{Mg}_2\text{Si}$  particles have an average  $D_e = 19.5 \pm 2.3 \mu\text{m}$  and aspect ratio near 1, while Cu-rich phases present important differences compared to the

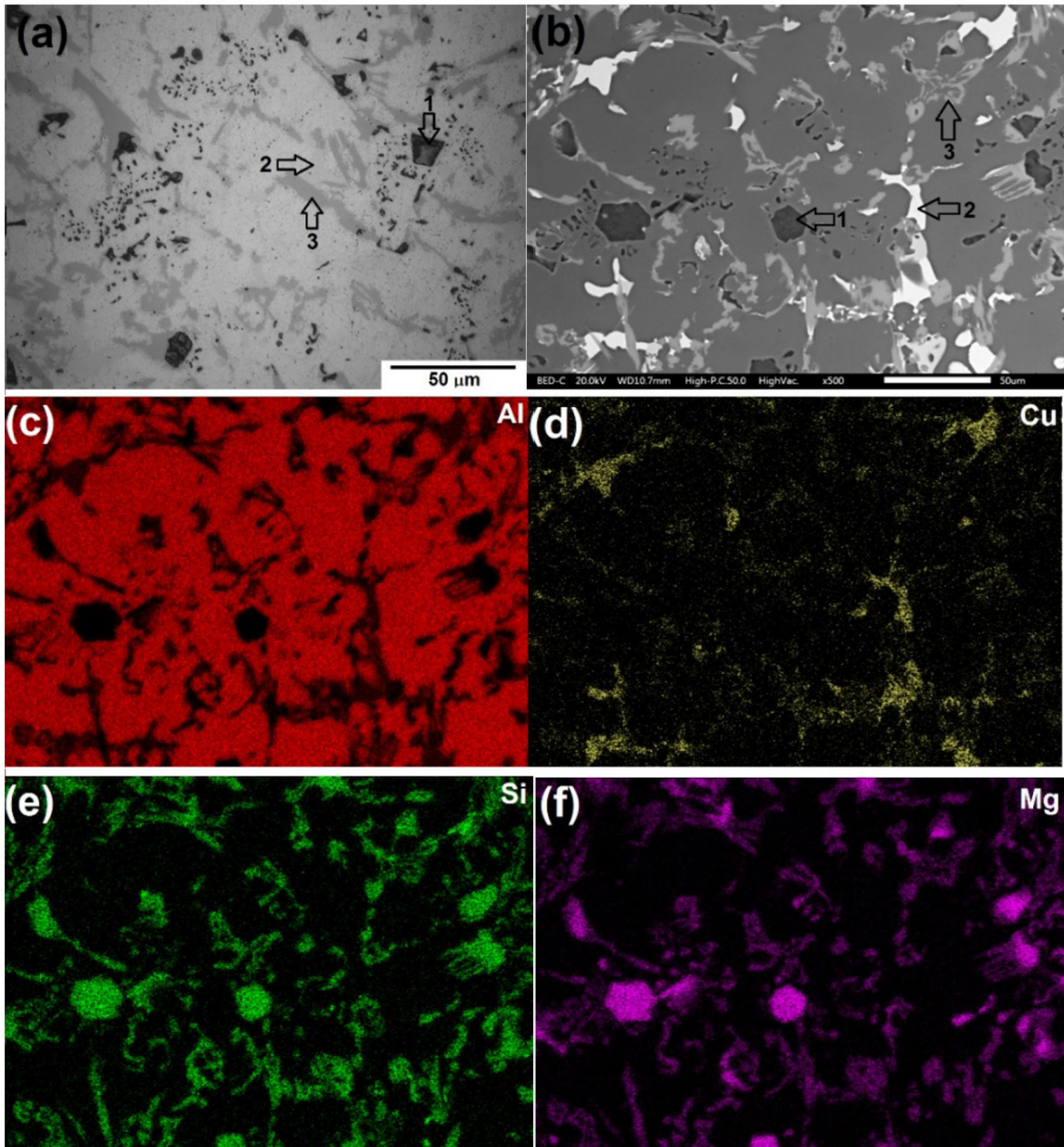


**Figure 4.** OM (a) and BE-SEM (b) micrographs of the experimental alloys with Cu content of 7%, and EDX-mappings corresponding to Al (c), Cu (d), Si (e) and Mg (f). Arrows indicate second phases: (1)  $\text{Mg}_2\text{Si}$ , (2)  $\text{Al}_2\text{Cu}$ , (3)  $\text{Al}_3\text{Cu}_2\text{Mg}_8\text{Si}_6$ , and (4) Si eutectic.

alloy Cu5 because for Cu7 their sizes are significantly smaller ( $D_e = 17.3 \pm 1.8 \mu\text{m}$  and aspect ratio of 1.3). The presence of second phases free zones is also observed, but with smaller average size ( $30 \pm 3 \mu\text{m}$ ) compared to alloy Cu5. No eutectic Si was observed. The microstructure obtained for this alloy was influenced by the increase in Cu content, although only the quantity of  $\text{Al}_2\text{Cu}$  increased compared to the alloy Cu5, decreasing Q. Besides, the quantity of  $\text{Mg}_2\text{Si}$  increased, and in this case is present mainly as primary particles. A plausible explanation for these results could be the above commented modification in Si:Cu:Mg ratio, 1:1.2:1.2 for the alloy with 7% Cu. This leads to Si:Cu and Mg:Cu ratios  $\leq 1$ , favoring  $\text{Al}_2\text{Cu}$  and reducing the quantity of Cu for Q formation (besides that primary  $\text{Mg}_2\text{Si}$  particles present higher content of Mg and Si than the eutectic Al-Mg<sub>2</sub>Si, reducing the quantity of these elements for Q formation). The analysis of the three different microstructures of the experimental alloys revealed that Si:Cu and Mg:Cu ratios higher than 2 favored  $\text{Mg}_2\text{Si}$  formation; ratios between 1 and 2 favored Q; and ratios lower than 1 favored  $\text{Al}_2\text{Cu}$ , which agrees with the observed in previous works<sup>1,5,25</sup>.

### 3.2 XRD analysis

Experimental alloys were analyzed using XRD to corroborate the phases already observed by OM and SEM, being presented in Figure 5 their diffractograms. As can be noted, the most important peaks correspond to  $\text{Mg}_2\text{Si}$ ,  $\text{Al}_2\text{Cu}$  and  $\text{Al}_3\text{Mg}_8\text{Cu}_2\text{Si}_6$ . A small peak for Si eutectic is observed just for the alloy Cu3, fact that can be explained due to the low quantity of this phase, as was above mentioned. For the alloy Cu3, Q and  $\text{Mg}_2\text{Si}$  are predominant, being barely visible  $\text{Al}_2\text{Cu}$  peaks. This result agrees with the images observed in previous figures. For the alloy Cu5 the increase in Cu

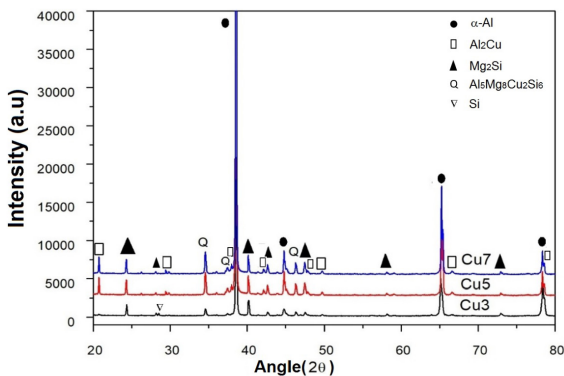


Figure 5. XRD diffractograms for the experimental alloys.

content led to obtain intense  $\text{Al}_2\text{Cu}$  peaks, remaining the intensity of Q and  $\text{Mg}_2\text{Si}$  peaks, not been appreciated peaks for Si. The X-ray pattern for the alloy Cu7 is very similar to Cu5, also coinciding with the phases observed in Table 2.

### 3.3 Microstructural fractal approach

Fractal analysis of these microstructures for the alloys with 3, 5 and 7% Cu revealed that  $D_f$  were respectively: i) 1.49, 1.60 and 1.59 for the whole microstructure; ii) 1.31, 1.55 and 1.45 for Cu-rich phases; and iii) 1.46, 1.17 and 1.26 for  $\text{Mg}_2\text{Si}$ . It can be noted the higher complexity of the microstructure for the alloys Cu5 and Cu7, fact that could be related to the higher quantity of second phases, which have different morphologies, and sizes bigger than for the alloy Cu3. The alloy with the lowest Cu content (Cu3) presented the lowest  $D_f$  value due to the presence of lower percentage of phases of smaller sizes. It is important to remember that larger the dimension  $D_f$ , the more heterogeneous and complex the image is<sup>21</sup>. Figure 6 demonstrates this fact, showing that patterns of big size have higher  $D_f$  than the same area composed by smaller phases.

For better mechanical properties there are desired rounded particles (e.g. spheres), which provide less stress concentration. This leads to the necessity of morphologies such as circles, or even Chinese scripts instead of elongated phases (e.g. needles)<sup>16</sup>. For aluminum alloys the fractal study of the whole microstructure has been reported in literature<sup>1,5,18,19</sup>, but no works were found which individually analyze the second phases. To reach this objective, each one of the second phases was analyzed not as a part of the whole microstructure but as an isolated feature. With the purpose of explain how a single phase could be studied from conventional and fractal points of view, a sequence of features is depicted in Figure 7. Taking into account that a solid circle has a fractal dimension  $D_f = 2.0$ , a value closed to 2 means a solid phase, while a decreasing value indicates that the phase could be similar to dendrites in crystals, Chinese scripts or fibrillar eutectics (see Figure 7, up). Besides, if a shape is elongated fractal dimension also decreases, meaning that its mass center is not compacted (Figure 7, down). This figure also presents the effect on  $R$  and  $F$ . The value of  $R$  can be the same for solid or irregular features, only depending on their aspect ratios (almost 1 for all the shapes in Figure 7, up). While in the case of  $F$ , as it depends on the perimeter, irregular forms significantly decrease their values. These data reveal the importance of combining these parameters because no one of them independently could characterize a complex phase. We are proposing their inclusion as a relative difference summation  $R + D_f + 2F$ , analyzing how far (in %) is a phase from a perfect circle ( $R + D_f + 2F = 5$ ), which is the highest

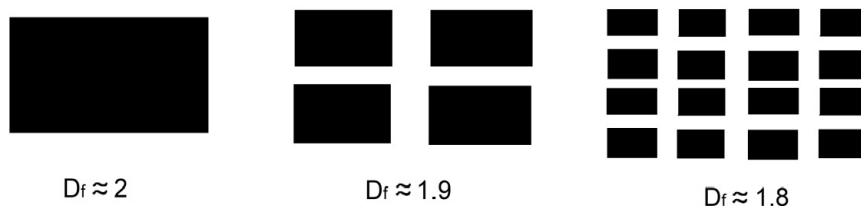
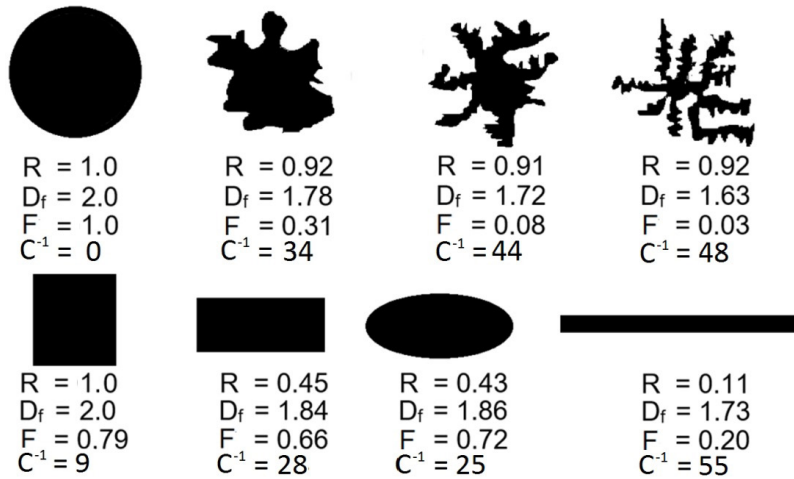


Figure 6. Effect of the size of objects with the same total area on fractal dimension.



**Figure 7.** Effect of different shapes on roundness, fractal dimension and shape factor.  $C^{-1}$  is also included, indicating how far a shape is from a perfect circle (in %).

possible value and the most desired in order to decrease localized stresses.  $F$  is multiplied by 2 because of the effect that it has for shapes with sharp corners, e.g. rectangles compared to ellipses. In Figure 7 it can be observed these relative differences, denoted as  $C^{-1}$ . The highest  $C^{-1}$  (55%) is for a needle like shape, which is the farthest from a circle and provides the highest stress concentration<sup>16</sup>.  $C^{-1}$  includes different characteristics, then not only differentiates between rounded and elongated shapes, but also between shapes with the same roundness, or with the same fractal dimension.

According to the above mentioned, Figure 8 shows examples of isolated phases and their average  $R$ ,  $D_f$ ,  $F$  and  $C^{-1}$  values for the experimental alloys studied in this work. These results show that phases present in the alloy with 5% of Cu have the shapes with highest  $C^{-1}$ , while the phases of the alloy with 3% Cu presented the lowest values. Comparing second phases individually, the order from highest to lowest  $C^{-1}$  were: Q, Al-Si, Al<sub>2</sub>Cu and Mg<sub>2</sub>Si, indicating that Q phase has the farthest shape from a circle, and Mg<sub>2</sub>Si the roundest one. These results could be useful for microstructural analyses, including the comparison between second phases, or possible correlations between alloying elements and the resulting second phases. In the case of this work, a direct correlation was not observed between Cu content modification and the values of  $C^{-1}$ . Future works could be also focused to comparatively analyze the values of  $C^{-1}$  for Si, Mg<sub>2</sub>Si, Al<sub>2</sub>Cu and Al<sub>5</sub>Cu<sub>2</sub>Mg<sub>8</sub>Si<sub>6</sub> in other alloys, also studying their response to heat treatments.

### 3.4 Compressive behavior

Compression test for the experimental alloys was carried out with the aim of show their behavior, for in future works analyze the possibility to obtain foams from these alloys through over-solution heat-treatment. Compared to the vast information found in literature for tensile behavior of Al alloys, for compression test this information is poor. Nevertheless, for Al foams is the inverse. This fact is explained due to their different applications, requiring to work under tension (Al alloys) or compression (Al foams). Figure 9 shows

the stress ( $\sigma$ ) vs. strain ( $\epsilon$ ) curves in compression for the experimental alloys. Please note that the compression test was carried out with the aim of demonstrating the behavior under compressive strain of the materials investigated. The compliance effect during the test was not subtracted; therefore, the obtained mechanical values are merely illustrative. Typical mechanical behavior is observed, with the elastic zones (maximized in Figure 9), plateaus corresponding to yielding, where materials begin to bulge outward on the sides and become barrel shaped. With increasing load, the specimens flattened out, offering increasing resistance to further shortening. From these curves it could be mentioned that mechanical behavior did not depend directly on Cu content but on the resultant microstructure. The formation of different second phases, with different percentages and shapes, leads to a difficult prediction of the mechanical behavior of the alloys, or to a difficult correlation between microstructure and mechanical properties. Nevertheless, it can be noted that the presence of bigger second phases free zones (soft  $\alpha$ -Al) and more elongated second phases for the alloy Cu5 could be a plausible cause of its lower strength. Otherwise, the higher strength for the alloy Cu7 could be originated by the presence of a higher quantity of hard second phases surrounding smaller soft second phases free areas. The inclusion of brittle second phases helps to obtain an increase in shortening at a higher rate than does the load<sup>26,27</sup>, while plastic strain of Al alloys is enhanced influenced by the increased volume fraction of ductile  $\alpha$ -Al solid solution and the lower amount of brittle intermetallic compounds<sup>28</sup>. In materials with hierarchical and/or complex microstructures there are reported both hardening and softening mechanisms, such as the works of Kim et al.<sup>28-30</sup>, which revealed high work hardening rates at initial stages of plastic deformation. These rates gradually decreased at larger deformations, even obtaining negative values after the middle of plastic deformation, which indicates work softening behavior and the modification of the dominant deformation mechanism. In this sense, in our alloys the soft  $\alpha$ -Al solid solution phase promotes the alloys to deform plastically, while the














|                        | Al <sub>2</sub> Cu   | Q  | Mg <sub>2</sub> Si   | Al-Si  | Average for each alloy  |
|------------------------|--|--|--|--|---|
| Cu3                    | <br>R = 0.73<br>D <sub>f</sub> = 1.60<br>F = 0.34<br>C <sup>-1</sup> = 40 | <br>R = 0.80<br>D <sub>f</sub> = 1.73<br>F = 0.21<br>C <sup>-1</sup> = 41 | <br>R = 0.94<br>D <sub>f</sub> = 1.80<br>F = 0.74<br>C <sup>-1</sup> = 16 | <br>R = 0.76<br>D <sub>f</sub> = 1.74<br>F = 0.33<br>C <sup>-1</sup> = 37 | R = 0.81<br>D <sub>f</sub> = 1.72<br>F = 0.41<br>C <sup>-1</sup> = 33 |
| Cu5                    | <br>R = 0.57<br>D <sub>f</sub> = 1.67<br>F = 0.37<br>C <sup>-1</sup> = 40 | <br>R = 0.51<br>D <sub>f</sub> = 1.51<br>F = 0.15<br>C <sup>-1</sup> = 54 | <br>R = 0.44<br>D <sub>f</sub> = 1.65<br>F = 0.22<br>C <sup>-1</sup> = 49 | <br>R = 0.52<br>D <sub>f</sub> = 1.74<br>F = 0.21<br>C <sup>-1</sup> = 46 | R = 0.51<br>D <sub>f</sub> = 1.63<br>F = 0.24<br>C <sup>-1</sup> = 47 |
| Cu7                    | <br>R = 0.89<br>D <sub>f</sub> = 1.76<br>F = 0.42<br>C <sup>-1</sup> = 30 | <br>R = 0.65<br>D <sub>f</sub> = 1.57<br>F = 0.24<br>C <sup>-1</sup> = 46 | <br>R = 0.97<br>D <sub>f</sub> = 1.74<br>F = 0.38<br>C <sup>-1</sup> = 31 | N/A  | R = 0.84<br>D <sub>f</sub> = 1.69<br>F = 0.35<br>C <sup>-1</sup> = 36 |
| Average for each phase | R = 0.73<br>D <sub>f</sub> = 1.68<br>F = 0.38<br>C <sup>-1</sup> = 37  | R = 0.65<br>D <sub>f</sub> = 1.60<br>F = 0.20<br>C <sup>-1</sup> = 47  | R = 0.78<br>D <sub>f</sub> = 1.73<br>F = 0.45<br>C <sup>-1</sup> = 32  | R = 0.64<br>D <sub>f</sub> = 1.74<br>F = 0.22<br>C <sup>-1</sup> = 42  |   |

Figure 8. Behavior of  $R$ ,  $D_f$ ,  $F$  and  $C^{-1}$  for each individual phase for the experimental alloys.

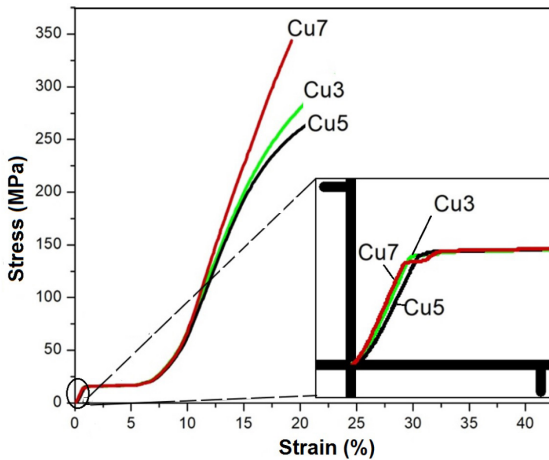


Figure 9. Compressive stress-strain curves for the experimental alloys.

higher hardness of the second phases leads to increase the strength of the alloys, which is directly proportional to the average hardness of the constituent phases<sup>28</sup>. For future works it is proposed the study of these alloys using other techniques such as thermal analysis and hardness. These new works will include an exhaustive in-situ analysis of the heat-treatment response of each second phase, including over-solution heat treatment at temperatures that could lead to their incipient melting. The information of second phases and mechanical behavior obtained in this work will help for a better understanding of this process.

#### 4. Conclusions

After the study of the effect of Cu content on the microstructure of experimental Al-6Si-xCu-7Mg (x = 3, 5 and 7 wt.%) alloys, the following conclusions can be written:

1. Second phases present in these alloys were: eutectic Si, Mg<sub>2</sub>Si, Al<sub>2</sub>Cu and Al<sub>5</sub>Cu<sub>2</sub>Mg<sub>8</sub>Si<sub>6</sub>. Their distribution, morphology and percentage depended on Cu content.
2. The increase in Cu content led to significant microstructural modifications, being the most important: i) increase in the percentage and size of second phases, mainly Cu-rich phases, with bigger zones free of second phases; ii) the quantity of Al<sub>2</sub>Cu increases; iii) eutectic Si formation decreases; and iv) microstructural complexity increased, defined by the increase in the value for fractal dimension.
3. A parameter denoted as  $C^{-1}$  which contains roundness, fractal dimension and shape factor was introduced for the analysis of how far a phase from a perfect circle is.
4. The alloy with intermediate Cu content (5%) presented the second phases with the shapes farthest from circles (highest  $C^{-1}$ ), while the lowest  $C^{-1}$  was for the alloy with 3% Cu.
5. Q phase presented the shape farthest from a circle (highest  $C^{-1}$ ), while Mg<sub>2</sub>Si the roundest one (lowest  $C^{-1}$ ).
6. The increase in Cu content did not directly affect the compressive behavior of the alloys, which

depended on the resultant microstructure. In this sense, the increase in the quantity of second phases and the presence of smaller zones with soft  $\alpha$ -Al led to increase the mechanical strength of the alloys.

## 5. Acknowledgements

This work was carried out with the support of the projects UNAM PAPIIT IN102719 and IN117316, and SEP-CONACTY 285215. H. Mecinas Eliezer is also acknowledged for his technical support in compression analysis.

## 6. References

- Alfonso I, González G, Lara G, Rodríguez M, Domínguez M, Téllez MG, et al. Fractal analysis of the heat treatment response for multiphase Al alloys. *Mater Res*. 2016;19(3):628-39.
- Medrano-Prieto HM, Garay-Reyes CG, Gómez-Esparza CD, Aguilar-Santillán J, Maldonado-Orozco MC, Martínez-Sánchez R. Evolution of microstructure in Al-Si-Cu system modified with a transition element addition and its effect on hardness. *Mater Res*. 2016;19(S1):59-66.
- Shaha SK, Czerwinski F, Kasprzak W, Friedman J, Chen DL. Effect of Cr, Ti, V, and Zr microadditions on microstructure and mechanical properties of the Al-Si-Cu-Mg cast alloy. *Metall Mater Trans, A Phys Metall Mater Sci*. 2016;47:2396-409.
- Samuel FH, Ouellet P, Samuel AM, Doty HW. Effect of Mg and Sr additions on the formation of intermetallics in Al-6 wt pct Si-3.5 wt pct Cu-(0.45) to (0.8) wt pct Fe 319-type alloys. *Metall Mater Trans, A Phys Metall Mater Sci*. 1998;29A:2871-84.
- Alfonso I, Figueroa IA, Béjar L, Gutiérrez HM, González G, Hernández O, et al. Characterization of Al-Si-Cu-Mg foams manufactured in-situ. *J Alloys Compd*. 2017;722C:797-808.
- Farina ME, Bell P, Ferreira CRF, Dedavid BA. Effects of solidification rate in the microstructure of Al-Si5Cu3 aluminum cast alloy. *Mater Res*. 2017;20(S2):273-8.
- Santos SF, Rodrigues JA. Correlation between fracture toughness, work of fracture and fractal dimensions of Alumina-mullite-zirconia composites. *Mater Res*. 2003;6(2):219-26.
- Sivarupan T, Caceres CH, Taylor JA. Alloy composition and dendrite arm spacing in Al-Si-Cu-Mg-Fe alloys. *Metall Mater Trans, A Phys Metall Mater Sci*. 2013;44:4071-80.
- Banhart J. Manufacture, characterisation and application of cellular metals and metal foams. *Prog Mater Sci*. 2001;46:559-632.
- García-Moreno F. Commercial applications of metal foams: their properties and production. *Materials (Basel)*. 2016;9:85.
- Rajak DK, Kumaraswamidhas LA, Das S. Technical overview of aluminum alloy foam. *Rev Adv Mater Sci*. 2017;48:68-86.
- Suarez MA, Figueroa IA, Gonzalez G, Lara-Rodriguez GA, Novelo-Peralta O, Alfonso I, et al. Production of Al-Cu-Fe metallic foams without foaming agents or space holders. *J Alloys Compd*. 2014;585:318-24.
- Jennings BR, Parslow K. Particle size measurement: the equivalent spherical diameter. *Proc R Soc Lond A*. 1988;419:137-49.
- Li M, Wilkinson D, Patchigolla K. Comparison of particle size distributions measured using different techniques. *Particul Sci Technol*. 2005;23(3):265-84.
- Kazakov AA, Kur A, Kazakova E. Development of quantitative methods for estimation of aluminum alloys structure by means of image analysis. *Microsc Microanal*. 2015;21:2111-2.
- Khomamizadeh F, Ghasemi A. Evaluation of quality index of A-356 aluminium alloy by microstructure analysis. *Sci Iran*. 2004;11(4):386-91.
- Krupiński M, Labisz K, Dobrzański LA, Rdzawski Z. image analysis used for aluminium alloy microstructure investigation. *J Achiev Mater Manuf Eng*. (Online). 2010;42:58-65.
- Durowoju MO, Akintan AL. Variation between fractal geometry and mechanical properties of Al alloys under different heat treatments. *International Journal of Advanced Science and Technology*. 2013;3:38.
- Jiang H, Lu Y, Huang W, Li X, Li M. Microstructural evolution and mechanical properties of the semisolid Al-4Cu-Mg alloy. *Mater Charact*. 2003;51:1-10.
- Perugini D, Poli G. Tourmaline nodules from Capo Bianco aplite (Elba Island, Italy): an example of diffusion limited aggregation growth in a magmatic system. *Contrib Mineral Petrol*. 2007;153:493-508.
- Mandelbrot BB, Passoja DE, Paullay AJ. Fractal character of fracture surface of metals. *Nature*. 1984;308:721-2.
- Liu C, Shi B, Zhou J, Tang C. Quantification and characterization of microporosity by image processing, geometric measurement and statistical methods: application on SEM images of clay materials. *Appl Clay Sci*. 2011;54:97-106.
- Rasband WS. ImageJ [Internet]. Bethesda, Maryland: U. S. National Institutes of Health; 1997 [cited 2019 Apr 13]. Available from: <http://imagej.nih.gov/ij/>
- Farahany S, Nordin NA, Ourdjini A, Abu Bakar T, Hamzaha E, Idris MH, Hekmat-Ardakan A. The sequence of intermetallic formation and solidification pathway of an Al-13Mg-7Si-2Cu in-situ composite. *Mater Charact*. 2014;98:119-29.
- Alfonso I, Maldonado C, Gonzalez G, Bedolla A. Effect of Mg content on the microstructure and dissolution of second phases in Al-Si-Cu-Mg alloys. *J Mater Sci*. 2006;41:1945-52.
- Liu L, Mohamed AMA, Samuel AM, Samuel FH, Doty HW, Valtierra S. Precipitation of  $\beta$ -Al5FeSi phase platelets in Al-Si based casting alloys. *Metall Mater Trans, A Phys Metall Mater Sci*. 2009;40A:2457-69.
- Jin HJ, Weissmüller J, Farkas D. Mechanical response of nanoporous metals: A story of size, surface stress, and severed struts. *MRS Bull*. 2018;43:35-48.
- Kim JT, Hong SH, Park JM, Eckert J, Kimet KB. Microstructure and mechanical properties of hierarchical multi-phase composites based on Al-Ni-type intermetallic compounds in the Al-Ni-Cu-Si alloy system. *J Alloys Compd*. 2018;749:205-10.
- Kim JT, Hong SH, Kim YS, Park HJ, Maity T, Chawake N, et al. Cooperative deformation behavior between the shear band and boundary sliding of an Al-based nanostructure-dendrite composite. *Mater Sci Eng A*. 2018;735:81-8.
- Kim JT, Hong SH, Park HJ, Kim YS, Suh JY, Lee JK, et al. Deformation mechanisms to ameliorate the mechanical properties of novel TRIP/TWIP Co-Cr-Mo-(Cu) ultrafine eutectic alloys. *Sci Rep*. 2017;7:39959.